Int. J. Multiphase Flow Vol. 10, No. 5, pp. 599–621, 1984
Printed in the U.S.A.

0301-9322/84 $3.00 + .00
Pergamon/Elsevier

FLOODING AND UPWARD FILM FLOW IN VERTICAL TUBES—II

SPECULATIONS ON FILM FLOW MECHANISMS

D. MOALEM MARON† and A. E. DUKLER
Chemical Engineering Department, University of Houston, Houston, TX 77004, U.S.A.

(*Received* 1 *January* 1983; *in revised form* 18 *October* 1983)

Abstract—Three mechanisms for flooding are suggested: (a) switching takes place between multiple stable states of the system, some of which cause upflow, (b) the system velocities exceed the propagation velocity of a kinematic wave and (c) entrainment carries liquid above the feed even with the liquid film flowing downward. The mechanism which is applicable in any case is the first one to come into effect as the gas rate is increased.

The idea of switching is also suggested as an explanation for the behavior of upward flowing films just above the flooding condition.

INTRODUCTION

Flooding in falling liquid films has been subjects of experimental and theoretical study for over 40 years. A wide variety of correlations have been proposed to explain this process where the liquid changes direction. These have been reviewed recently by Dukler & Smith (1977) and Tien & Liu (1979). In general the approaches are based either on dimensional analysis with experimental data used to fit the constants or on physically unrealistic mechanisms. Comparisons with data show they are unable to predict flooding under conditions significantly different from the ones used to construct the correlations in the first place. In this paper new processes for flooding and flow reversal are suggested based on the mechanics of unsteady film flow. The large waves which exist on the surface of falling films are shown to be a causative factor in the process but not the primary mechanism by which reversal takes place.

SOME POSSIBLE MECHANISMS

Consider a falling liquid film with countercurrent gas flow in a vertical tube. The liquid feed enters the tube somewhere along its length through a porous sinter with the top and bottom of the tube being the two limiting locations. At low gas rates all of the liquid falls as a film as in figure 1(A) and the gas liquid interface is covered with waves. With increasing gas rate a point is reached where drops and film are observed above the level of the feed. This is always accompanied by a sharp increase in waviness on at least part of the liquid film falling below the feed. With the feed located at the top of the column as in figure 1(B), the result will be the initiation of flooding. However, if a section of tube is located above the feed as in figure 1(C), then the droplets lifted above the feed deposit on the wall and form a film which falls. For short tube lengths it is possible to observe flow out the top since the tube is not long enough to effect complete deposition. For longer lengths the deposition will be more complete and negligible carryover out the tube will take place. Then in order to reach the point of flooding, the gas rate must be increased until the interfacial shear is sufficient to lift the film. As shown in figure 1(D), flooding takes place for this type of system with liquid flowing upward as a film and as droplets. Further increases in gas rate result in increasing fractions of the feed liquid flowing upward until a gas rate is reached at which no liquid flows downward at all.

The condition of flooding is always accompanied by a sharp rise in the axial pressure gradient in the sections of tube both above and below the feed. This rise is not gradual

†Present address: Department of Fluid Mechanics and Heat Transfer, University of Tel-Aviv, Tel-Aviv, Israel.

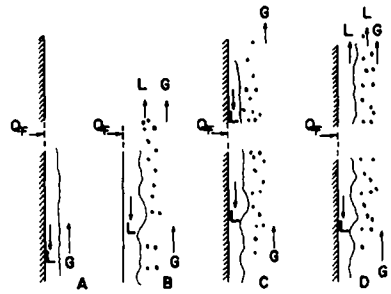

Figure 1. Various conditions for flooding.

with increases in gas rate. Rather, one observes a sharp discontinuity for each liquid rate as a critical gas rate is exceeded.

Three possible mechanisms have been suggested by which flooding as described above can take place: (A) Wave motion; (B) Entrainment; and (C) Film flow.

(A) *Wave motion.* The suggestion first made by Hewitt & Wallis (1963) that flooding is caused by large waves on the interface has been widely accepted. The argument which led to this idea has two parts.

- The initiation of flooding is always accompanied by the appearance of large waves somewhere along the interface on the film below the feed.
- If one *calculates* the velocity distribution in the smooth falling film using the measured pressure drop to obtain the interfacial shear, the interfacial film velocity is determined to be downward just below the gas flow rate at which flooding takes place. Thus, it was concluded that flow in the film cannot be responsible for the flooding and the mechanism must be related to the presence of the waves.

Conceptually, the appearance of a large wave cannot account for the flooding process unless there is a mechanism by which the liquid in the wave is lifted above the feed. Two such mechanisms have been suggested.

(1) Once a finite amplitude wave is formed, it continues to grow until it bridges the tube and the liquid is then carried up as a slug or as an entrained phase. Fundamental to this mechanism is the concept that the gas velocity needed to lift the drops or slugs once formed from the wave is less than the velocity needed to generate wave growth. Perhaps this idea had its origin in the work of Schutt (1959). He explored the stability of the liquid film using Orr–Summerfield analysis to find the interfacial shear at which waves would grow. It was assumed that once the growth was initiated the process would continue until bridging occured. His calculated shear rates at flooding were not in agreement with experiment.

Shearer & Davidson (1965) calculated the amplitude and shape of a standing wave by assuming gravity and surface tension were balanced by the impact pressure due to gas flow. They calculated the gas rate at which the wave becomes very large and thus presumably results in bridging. Agreement with data at a variety of conditions was poor. A recent approach to this idea of a wave growth mechanism for flooding was presented by Zvirin *et al.* (1979).

Suggestions that bridging takes place have appeared repeatedly in the literature over the past 15 years, with recent examples being that of Imura *et al.* (1977) and Duffy *et al.* (1978). However, measurements of the maximum film thickness as illustrated in figure 11, part I and by Suzuki & Ueda (1977) convincingly demonstrate that bridging simply does not occur. Some photographic evidence (Hewitt & Whalley 1980) suggests that for high liquid flow rates occasional bursting of a large wave takes place to form a locally dense droplet phase which is carried upward by the gas. However, under other conditions such as those discussed in part I, at low liquid rates no such bursting takes place. When flooding

takes place in large tubes, the possibility of bridging must be rejected simply from a consideration of the amount of liquid necessary to fill the tube compared to the small amount of liquid flowing in the film.

(2) The large waves which are formed are kinematic, thus carrying mass. As a result of shear and/or form drag from the gas, these waves are propagated upward and carry the liquid past the feed point resulting in flooding. In order to predict the conditions for flooding for this model, it is necessary to determine the gas rate at which the wave will just become stationary. At gas rates greater than this value flooding will take place. Cetinbudaklar & Jameson (1969) attempted to predict the gas velocity at which an unstable standing wave would develop by the use of a stability analysis of the Schutt type. It is assumed that at higher gas velocities the waves would move upward, hence flooding would take place. However, careful observations show that flooding can take place under conditions where the waves flow downward. It is a curious fact that no measurements have been reported of the velocity of these large waves as the condition of flooding is reached. Hewitt & Wallis (1963) report on the velocity of the falling waves and show that there is little or no influence of the counterflow air. However, these measurements were not carried out for air rates which approached the flooding conditions.

It must be concluded that despite its wide acceptance, the evidence that the flooding process is connected in a primary way with the wave motion or growth is purely circumstantial.

(B) *Entrainment.* The appearance of entrained drops at or just below the gas rate at which flooding takes place suggests a second possible mechanism. In this case the waves play the role as the source of entrainment. Flooding takes place when the gas rate is sufficient to lift the largest drops upward against gravity. Underlying this concept is the idea that the gas velocity necessary to form the large waves and to tear off the droplets is less than that necessary to lift the largest drops out of the tube. Thus, in order to predict entrainment it is necessary to explore the drop mechanics rather than the wave mechanics.

The objective in this approach is to calculate the minimum gas velocity needed just to suspend the largest stable drop. A balance between the drag due to gas flow around the drop and gravity acting on the drop produces the relationship needed for gas velocity in terms of an unknown drop diameter. But this maximum stable drop size can be expressed in terms of a critical Weber number and the result is then

$$\bar{U}_G = \left[\frac{4\mathrm{We}_c}{3C_d}\right]\frac{[\sigma g(\rho_L - \rho_G)]^{1/4}}{\rho_{G^{1/2}}} \qquad [1]$$

where g is the acceleration due to gravity, σ is the liquid surface tension, ρ_L and ρ_G are the densities of the liquid and the gas, C_d is the drag coefficient, We_c is the critical Weber number, and $\bar{U}_G$ is the true mean gas velocity which is related to the superficial velocity U_G' through the voids, $U_G\alpha = U_G'$. For the gradual accelerations which occur when a drop is formed from the wave (near the flooding condition), $\mathrm{We}_c = 30$ (Sevik & Park 1973). Furthermore, for large drops $C_d \simeq 0.44$. With these substitutions one obtains

$$U_G' = 3.1\frac{[\sigma g(\rho_L - \rho_G)]^{1/4}}{\rho_{G^{1/2}}}\alpha \qquad [2]$$

Now consider the case of low liquid rates or large diameter tubes where α approaches 1.0; the result is identical in form to the flooding correlation recommended by Pushkin & Sorokin (1969), (sometimes called the Kutateledze correlation) with the constant they suggested being 3.2. Considering the fact that Pushkin's correlation was derived from

dimensional analysis and experiment and that the above equation came completely from a theoretical model, the agreement is remarkable. Furthermore, this model is in good agreement with the data of part I of this paper and with the results of Hewitt (1977) for various fluid properties and tube sizes.

Notwithstanding the success of [2] for these conditions of test, other measurements have shown that the Kutateladze equation does not describe the true behavior under a variety of conditions. Because of its close correspondence with Kutateladze, this model will also fail under those conditions. Furthermore, when studied in detail, this entrainment model predicts unreasonably large drop sizes under those same conditions. Thus, it clearly is not a fully general model for the flooding mechanism, although this mechanism for flooding is likely to exist under certain circumstances.

(C) *Film flow.* The possibility of upward flow in the film as a mechanism of flooding seems to have received comparatively little attention in the literature until recently since this idea was rejected by Hewitt & Wallis (1963). Some tentative and inconclusive explorations in a related study of upward annular film flow are reported by Nicklin & Koch (1969). Solevev *et al.* (1967) integrated the momentum equations for smooth laminar film flow for the conditions of upward gas flow and both upward and downward film flow. The result was a relationship between the shear stress at the wall and interface, the pressure gradient, the film flow rate and film thickness. The solution displayed two branches, one for concurrent and one for countercurrent upward flow which approaches each other asymptotically. It was suggested that the location of the asymptote characterized the flooding point, but no physical basis was presented for this premise and the detailed data on film thickness and shear of part I show the premise to be invalid.

Richter (1981) as well as Taitel *et al.* (1982) present steady state film models for smooth films. Both leave questions as to the mechanics of flow at flooding and their results depend strongly on the form of the curve fit to experimental interfacial shear and/or wave characteristics.

In this paper the concept of an unsteady state mechanism for flooding is explored along with the idea that large waves which are observed at the flooding condition are the result not the cause of the actual process of upflow in the film.

A THEORETICAL ANALYSIS OF FILM FLOW

The momentum equations and reference states. For an incompressible, Newtonian fluid the equation for steady, laminar, one dimensional motion is

$$\frac{\mu_L}{\rho_L}\frac{\partial^2 u}{\partial y^2} + \phi g = 0 \qquad [3]$$

where

$$\phi = \frac{g - \dfrac{1}{\rho_L}\dfrac{dp}{dx}}{g},$$

g and dp/dx are the acceleration due to gravity and the pressure gradient in the downward, x direction, y is the coordinate direction normal to and measured from the wall, while ρ_L and μ_L are the density and viscosity of the liquid, and u is the local velocity in the film. The liquid interface is known to be highly wavy as discussed above, and this wave action increases as the condition of flooding is reached. However, in order to explore the *film mechanism* for flooding, [3] is applied to a liquid film whose interface is assumed to be smooth. This is equivalent to the assumption that the effect of the wave motion on the

velocity in the film averages out over time and position as if the film remained smooth. The fact that the measured mean film thickness is about equal to the theoretically calculated one below the flooding point (see figure 8 of part I) suggests this may be a reasonable assumption. However the condition above flooding may be very different as will be discussed subsequently. As difficult as it is to accept this concept in view of recent studies (see Dukler 1977) it is necessary to take this approach to fully test the film mechanism.

Using [3] we explore the existence of certain reference states of the film which can be physically meaningful in understanding the mechanism of flooding (see figures 2–4).

- The "*N* State": the free falling film.
- The "*O* State": the falling film with zero velocity at the interface. This represents a limiting condition for uniform downflow. Higher interfacial velocities result in upflow at some point in the film.
- The "*U* State": the rising film with zero velocity gradient at the wall. This represents a limiting condition for uniform upflow. Lower interfacial velocities will result in downflow at some point in the film.

As will be seen, many other states can exist but they can all be viewed in relation to these reference states.

In most practical cases the pressure gradient is negligible compared with $\rho_L g$ and $\phi \to 1.0$. For vertical flows, assuming no-slip at the wall where $y = 0$ and zero shear stress at the liquid–gas interface, the Nusselt velocity profile is obtained, which by further integration over the film thickness yields the Nusselt film thickness, δ_N,

$$\delta_N = \left(3Q_L \frac{\mu_L}{\rho_L g}\right)^{1/3} \qquad [4]$$

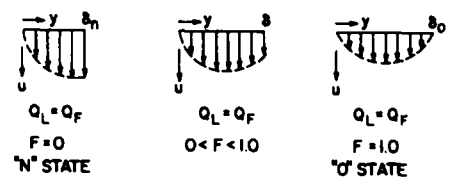

Figure 2. Velocity distributions for uniformly downflow.

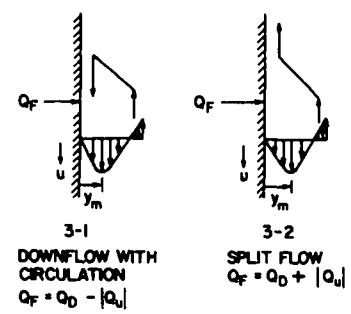

Figure 3. Film flow with velocity reversal in the film.

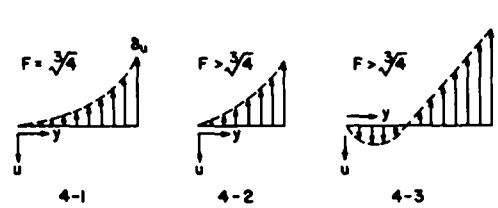

Figure 4. Upflow in the film with $Q_L = -Q_F$.

where Q_L is volumetric flow rate in the film per unit perimeter and equals the external liquid feed rate per unit perimeter, Q_F.

If upward gas flow takes place counter to the falling film, the velocity profile is distorted in such a way that the local downward velocity near the interface is reduced due to the gas shear. With sufficient opposing shear, the velocity at the interface approaches zero. Under this condition of zero interfacial velocity, the velocity profile is

$$u = \frac{\rho_L \phi_0 g}{\mu_L} \frac{1}{2}(\delta_0 y - y^2) \qquad [5]$$

where δ_0 is the film thickness at this state. This thickness can be determined by integrating [5] over the thickness δ_0 to yield

$$\delta_0 = \left(12 Q_L \frac{\mu_L}{\rho_L \phi_0 g}\right)^{1/3}. \qquad [6]$$

Using [5] to obtain the velocity gradient, it is seen that the interfacial shear stress at this point is

$$\tau_0 = -\frac{\rho_L \phi_0 g \delta_0}{2}. \qquad [7]$$

With further increases in interfacial shear the velocity close to the interface can, in principle, reverse and partial upflow results. If the shearing effect is large enough, the U state is reached where the shear is just sufficient to lift all of the liquid in the film. At this point the shear stress at the wall is zero, the film thickness is δ_u and the upflow velocity profile is given by

$$u = -\frac{\rho_L \phi_u g}{\mu_L} \frac{y^2}{2} \qquad [8]$$

which by integration yields

$$\delta_u = \left(6 Q_L \frac{\mu_L}{\rho_L \phi_u g}\right)^{1/3}. \qquad [9]$$

The interfacial shear needed to reach this state is

$$\tau_u = -\rho_L \phi_u g \delta_u. \qquad [10]$$

Some comparisons are useful:

$$\frac{\delta_u}{\delta_N} = \sqrt[3]{2/\phi_u} \qquad \frac{\tau_u}{\tau_0} = \left(2\frac{\phi_u}{\phi_0}\right)^{2/3}$$

$$\frac{\delta_0}{\delta_N} = \sqrt[3]{4/\phi_0} \qquad \frac{\delta_0}{\delta_u} = \left(2\frac{\phi_u}{\phi_0}\right)^{1/3}.$$

It is of interest to explore the velocity distribution and film thickness for states other than the three reference states for arbitrary values of interfacial shear. Because there is still insufficient information to relate the shear to operating variables, it is convenient to make

these calculations in terms of the shear. As will be shown, given a value of the shear there exist multiple solutions to the equations for film flow for certain ranges of shear stress.

General solution of the flow equations. Define the interfacial shear τ_i, in terms of its multiple of τ_0 at the zero state

$$F \equiv \tau_i/\tau_0 = -\frac{2\tau_i}{\rho_L \phi_0 g \delta_0} \qquad [11]$$

Integration of [3] then produces the velocity distribution for the general case

$$u = \frac{\rho_L \phi g}{\mu_L}\left[\left(\delta - \sqrt[3]{0.5}\, F\delta_N \frac{\phi_0^{2/3}}{\phi}\right)y - \frac{y^2}{2}\right]. \qquad [12]$$

Note that $u > 0$ indicates downflow while $u < 0$ designates upflow. Integration of the velocity over the film thickness δ, yields

$$Q_L = \frac{\rho_L \phi g \delta^3}{3\mu_L}\left(1 - \frac{3}{4}\sqrt[3]{4/\phi_0}\frac{\delta_N}{\delta}F\right) \qquad [13]$$

Q_L is the liquid flowing along the wall. The feed is introduced somewhere between the top and the bottom of the column at a rate Q_F. In the absence of interfacial shear when all liquid is flowing down $Q_L = Q_F$. If the shear is high enough so that all the flow is upward, then $Q_F = -Q_L$. Between these two cases there are a variety of possibilities as will be demonstrated in what follows:

(A) *Uniformly downflow* ($0 \le F \le 1$; $u \ge 0$, $Q_L = Q_F$). This situation is pictured in figure 2 where for all values of y, the velocity is always positive, or downward directed. Since $Q_L = Q_F$, it is possible to normalize [13] using [4] to obtain

$$R_N^3 - 0.75\sqrt[3]{4}\, R_N^2 \frac{\phi_0^{2/3}}{\phi}F - \frac{1}{\phi} = 0 \qquad [14]$$

where $R_N = \delta/\delta_N$, the normalized film thickness. In the range $0 \le F \le 1$ this cubic equation has only one real root and the solution for R_N is shown as curve N–O in figure 5 for the case of $\phi = 1.0$. The data reported in part I of this paper show that ϕ is seldom less than 0.95. For values of $\phi < 0.9$ the results will be negligibly different from those reported in figure 5.

(B) *Downflow with circulation* ($F \ge 1$, $u_L \gtrless 0$, $Q_L = Q_F$). As the shear is increased past reference state 0, the distribution can shift so that the velocity at the outer portion of the film changes direction to upflow. When that happens there are two possibilities as illustrated in figure 3. In figure 3–1 the portion of the film where $u < 0$ flows up above the feed. However, the shear induced by the gas is insufficient to lift the liquid as a rising film. This is equivalent to the situation pictured in figure 1(C). Under these conditions the net liquid flowing down is Q_F, but the liquid flowing upward falls back and adds to the liquid feed as an internal recycle. The velocity distribution for this condition is described by [12] and [14] is equally valid. The solution for this case given as curve OB in figure 5.

Designate y_M the distance from the wall to the plane of zero velocity gradient. Then the amount flowing down Q_D and up Q_u, in the the film are

$$Q_D = \int_0^{2y_M} u\, dy = \frac{2}{3}\frac{\rho_L \phi g}{\mu_L} y_M^3 \qquad [15a]$$

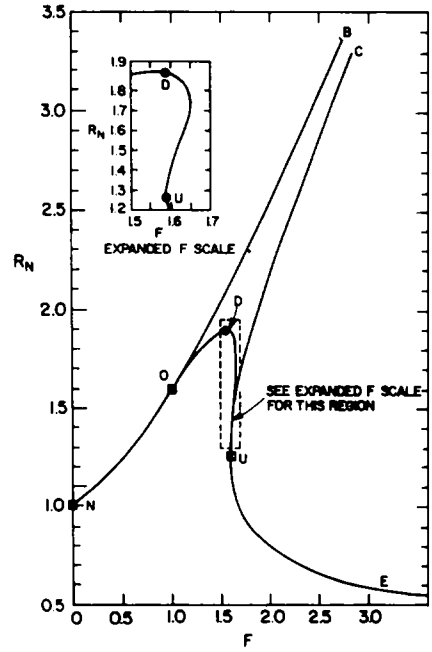

Figure 5. Dimensionless film thickness variation with dimensionless interfacial shear.

$$Q_u = \int_{2y_M}^{\delta} u \, dy = \frac{\rho_L \phi g}{\mu_L}\left[-\frac{2}{3}y_M^3 + \frac{1}{2}y_M\delta^2 - \frac{\delta^3}{6}\right] < 0 \qquad [15b]$$

$$y_M = \delta - \sqrt[3]{0.5}\,\frac{\phi_0^{2/3}}{\phi} F\delta_N. \qquad [15c]$$

Equation [15c] for y_M is obtained from the condition that at $y = y_M$, $du/dy = 0$. For the case of downflow circulation illustrated in figures 3(A) and 1(C), the material balance over the film requires that

$$Q_L = Q_F = Q_D - |Q_u|. \qquad [16]$$

(C) *Split flow* ($F \geq 1.0$, $u_L \gtrless 0$, $Q_L/Q_F \leq 1.0$). Figure 3–2 demonstrates this situation. As in Case (B), the velocity in the liquid is downward near the wall but reverses in the film near the interface. However, splitting takes place when the shear due to gas flow is sufficient to prevent that liquid which rises above the feed to fall back and circulate. When this takes place the material balance requires

$$Q_F = Q_D + |Q_u|. \qquad [17]$$

Substituting for Q_D and Q_u using [15] and then normalizing with [4] gives the relationship

$$R_N^3 - \frac{7F}{2}\sqrt{0.5}\,\frac{\phi_0^{2/3}}{\phi} R_N^2 + 4F^2\sqrt[3]{0.25}\,\frac{\phi_0^{4/3}}{\phi^2} R_N - \frac{1}{3}\left[2F^3\frac{\phi_0^2}{\phi^3} + \frac{1}{\phi}\right] = 0. \qquad [18]$$

The solution to this equation for $\phi = 1.0$ is shown in figure 5 as the curve O–D–U. A portion of the solution is shown in the insert with an expanded F scale. It is important to note that (for $\phi = 1.0$):

- Solutions to this equation exist only over the region $1 \leq F \leq 1.67$.
- The maximum possible value of R_N is 1.89.

• In the region $\sqrt[3]{4} < F < 1.67$, for each F, two physical real solutions exist (see insert with expanded F scale). These correspond to two velocity distributions which satisfy the force balance and thus, two pairs values of Q_u and Q_D.

Thus, if the mechanisms for flooding involves splitting of the flow, then it can take place only under the range $1 \leq F \leq 1.67$. However, as seen from figure 5, if $1 < F < \sqrt[3]{4}$, two values of R_N are possible; one if the flow splits as shown from the curve O–D and one if the flow recirculates as given by the solution O–B. If the conditions are such that $1.587 < F < 1.67$, then three solutions for R_N are possible, two if the flow splits as given along the curve D–U and one if there is recirculation, as given by O–B.

It is important to understand the physical concepts involved in development of [18]. Equation [14] has been reported previously in the literature (Feind 1960) although the relationship between Q_L, Q_u and Q_D, and especially the multiple solutions, has not been made clear. However, [18] represents a new solution to this problem never before reported. It cannot be obtained by direct integration of the velocity distribution because it requires that the upflow and downflow be uncoupled as implied by [17].

(D) *Upflow* ($F > \sqrt[3]{4}$, $u \gtrless 0$, $Q_L = -Q_F$). A general relationship between R_N and F can be obtained from [13] by recognizing that for upflow $Q_L = -Q_F$. Then [13] can be normalized by δ_N through [4] to obtain

$$R_N^3 - 0.75\sqrt[3]{4}\, R_N^2 \frac{\phi_0^{2/3}}{\phi} F + \frac{1}{\phi} = 0. \qquad [19]$$

In contrast to [14] for uniform downflow which has only one real root, this equation can be shown to have three real roots, one of which is negative and thus nonphysical. The solution to this equation for $\phi = 1.0$ appears as curve EUC in figure 5. The EU branch represents uniform upflow (figure 4–2). The UC branch is upflow circulation (figure 4–3). The branch point, U, is the limiting case (figure 4–1). At a value of $F = \sqrt[3]{4}$, [18] for split flow displays two solutions for R_N, one of which is the value of R_u as predicted by [19].

As F becomes sufficiently large the downflow and upflow circulation curves beome asymptotic to each other. The asymptotic curve (evaluated from either [14] or [18] at large F) is:

$$R_N = 0.75\sqrt[3]{4}\, F \text{ or } \tau_i = \frac{2}{3}\rho_L g \delta \phi. \qquad [20]$$

This is identical to the criterion used by Solevev (1967) for the onset of flooding. Now it is possible to see that the physical mechanism implied by Solevev's criterion is that flooding takes place when the flow switches from downflow circulation to upflow circulation. As will be shown below, flooding takes place at conditions very different from this one.

A comparison of film flow mechanisms. Each of the mechanisms A–D discussed above controls the characteristics of the flow. Figure 5 shows the variation of dimensionless film thickness with dimensionless interfacial shear. Figure 6 displays the liquid flowing down, Q_D, relative to the feed, Q_F, as a function of F for each model. Along the line N–O, all the liquid falls. Along curve O–D, splitting of the flow takes place with the amount flowing downward decreasing with increasing shear until the two streams are equally split at point D where $F = \sqrt[3]{4}$. The curve O–B represents downflow with circulation. For $F > 1.0$ the internal circulation causes the liquid falling below the feed to exceed Q_F. In a similar way, if the mechanism is upflow circulation, the liquid near the wall in downflow could result in Q_D/Q_F varying with F as shown in curve U–C. Of course, for uniformly upflow Q_D is zero as shown along the curve U–E.

Of particular interest are the curves for the wall shear stress normalized by the shear

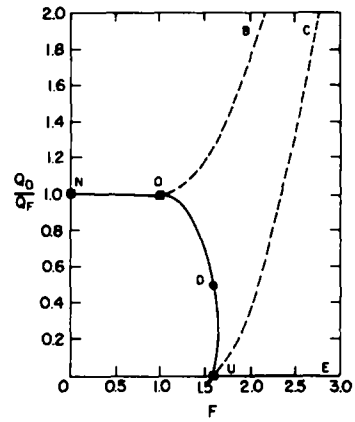

Figure 6. Distribution of feed with interfacial shear.

stress at the wall for a free falling film, τ_{WN}. These are shown in figure 7. The results suggest that dynamic wall shear stress measurements would be a useful tool to discriminate between the mechanisms which actually exist.

FILM FLOW AND FLOODING

In this paper two new mechanisms for flooding are suggested, both based on the existence of film flow: (A) Switching between steady state solutions, and (B) Limiting kinematic wave propagation velocity. The model which controls for any given condition is the one which exists at the lowest gas flow rate, or is the lowest of the transition conditions.

(A) *Switching model*

This process is pictured as a dynamic one with the instantaneous interfacial shear, the film thickness, velocity distribution and in some cases flow direction oscillating with time. Furthermore, it is suggested that the apparent presence of the large waves on the film at flooding is the result of switching between different states of the system having different film thicknesses.

At zero gas flow the liquid moves down the wall as a film with the surface covered by a stable wave structure. With increasing countercurrent gas rate the wave amplitude as

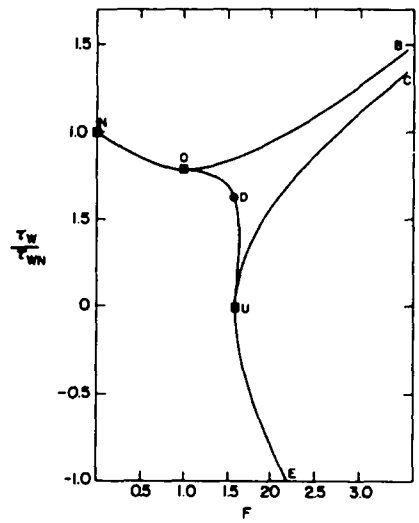

Figure 7. Wall shear stress variation with for the various models.

indicated by the RMS film thickness (figure 13, part I) increases but not enough to have a significant effect on pressure gradient or thus on τ_i or F. As the gas rate for flooding is approached, the wave amplitude increases dramatically and two events take place: (1) the interfacial shear increases markedly causing a step change in F; and (2) entrainment starts (figure 6, I). If this change causes F to exceed 1.0, then multiple states can exist in the film. For example, with an increase in F into the range $1 < F < \sqrt[3]{4}$ the film thickness can oscillate locally between the solutions given by curves O–B and O–D of figure 5. Thus, it would *appear* as if large waves are formed and move up the film but, in fact, the film thickens and flows are controlled by the solutions to the film equations.

Increased gas rates are not necessarily accompanied by increased shear stress, but rather by a change in the fraction of time each state exists. If the jump in shear takes place such that $\sqrt[3]{4} < F \leq 1.67$, then the system can oscillate between three states, two along branch DU and one along OB.

An alternate speculation involves the possibility of a limit cycle. Figure 8 demonstrates this model. At gas rates below the flooding point F remains low, say, at point 1. Once the gas rate causes growth of the existing wave structure, F increases drastically to point 2. The film thickness increases but so does the interfacial shear as a result of the thicker film and F jumps to position 3. At this state the film thins resulting in decreased shear and F goes to point 4. If the conditions at 4 generate a shift in F to point 2, then the limit cycle is generated.

It remains to understand the driving force for this process of switching. One possibility is the entrainment carried by the gas. These large drops, frequently larger than the mean film thickness, moving with velocities much higher than the liquid provide the needed source of mass, energy and momentum for changing from one state to the other.

It is important to understand the difference between this model and a wave model for flooding. Both are initiated by growth of already existing waves but the mechanism for reversal is completely different and models for predicting the distribution between up and downflow would likewise be different. In the wave model the increased gas rate causes the waves at the interface to grow. Then they eigher become large enough to bridge the tube and the liquid is forced upward as a slug or the large waves propagate upward along the film. As pointed our earlier, evidence for bridging or upward flow of the waves is meager. In the film model the increased wave amplitude causes a sharp increase in interfacial shear. The high shear causes upflow by shifting the film to a condition at which multiple states are possible, some of which result in net upflow. If the states are unstable ones, then the observed film thicknesses would oscillate between these possible states with the peaks and valleys of the surface profile representing the various possible states for film flow. The rate of upflow of the liquid would be determined from solutions of the film equation and some knowledge of the distribution of time between these states rather than from solutions of the equations of motion for large roll waves which are, as yet, poorly understood.

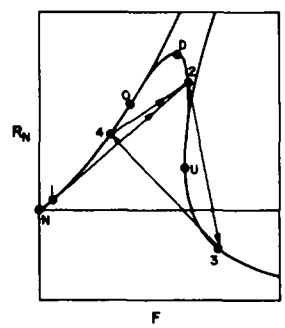

Figure 8. A limit cycle in film flow.

Qualitative evidence which appears to support these speculations have been developed from an analysis of the time varying film thickness and pressure gradient data of part I.

Mean and RMS film thickness. Table 1 summarizes some data on the mean and RMS fluctuation in interfacial shear and film thickness at the flooding point for the four experimental feed rates described in part I, test section configuration *B*. At each of the transitions the measured pressure gradient and film thickness were used to calculate τ_i and F using

$$\tau_i = -\frac{dP}{dx}\frac{(D-2\delta)}{4} \qquad [21]$$

and [11] for F. The RMS fluctuating gradient was similarly translated into an RMS fluctuation in F, F_{RMS} and this was used to characterize the range of the variation in F as F_{RMS}. Corresponding tabulated values of R_N and $(R_N)_{RMS}$ were calculated from experimental values of δ and δ_{RMS} at the flood point using $R_N = \delta/\delta_N$.

Consider $Re_F = 310$. At the flood point the range of F is 1.58–2.48. In order to compare with theory these values of F are used to predict R_N and $(R_N)_{RMS}$ and these are compared with data. The switching process is pictured as follows. Just below the flood point there is an increase in surface roughness and F increases to 1.58. Entrainment takes place, deposits liquid above the feed which falls and establishes a downflow circulation. The film thickens to satisfy a solution along curve OB and displays a value of $R_N = 2.17$ for $F = 1.58$. However, when the film thickens a sharp increase in interfacial shear takes place and F increases to $F = 2.48$. There simply is not enough liquid inventory to permit further thickening of the film along curve OB so the system switches to another solution along curve UE where $R_N = 0.67$. As the film thins the shear decreases to 1.58 again and the process continues. Of course, intermediate states are possible as will be discussed below, but for a simple qualitative picutre this two point switching is presented. A simple theoretical mean value of R_N would be the arithmetic average of the two states or $R_N \simeq 1.42$. Some measure of the fluctuation would be the difference between the mean and each state or $(R_N)_{RMS} \simeq 0.75$. These are seen to agree quite well with corresponding experimental values for the two lowest feed rates, $Re_F \simeq 310$ and 776.

Table 1. Comparison of normalized mean and RMS film thickness at the flooding transition

	LIQUID FEED REYNOLDS NUMBER					
	310	776	1552		3105	
	DATA					
VALUES BASED ON Q_F						
F	2.03	1.73	0.88	1.52	0.59	1.01
F_{RMS}/F	0.22	0.19	0.26	0.19	0.30	0.25
RANGE OF F	1.58 - 2.48	1.41 - 2.05	0.65 - 1.14	1.23 - 1.81	0.29 - 0.89	0.75 - 1.25
R_N	1.59	1.48	1.02	1.19	1.03	0.92
$(R_N)_{RMS}$	0.73	0.67	0.50	0.52	0.53	0.40
Q_D/Q_F	1.00	1.00	0.96	0.56	0.93	0.31
VALUES BASED ON Q_D						
RANGE OF F				1.49 - 2.19		1.11 - 1.85
R_N				1.44		1.36
$(R_N)_{RMS}$				0.64		0.56
	THEORY					
R_N	1.42	1.40		1.40		1.28
$(R_N)_{RMS}$	0.75	0.68		0.65		0.44

The existence of two flooding type transitions for the higher flow rates was discussed in part I. Clearly this switching mechanism cannot apply at the first transition since, as shown in the table $F < 1.0$ at flooding and under this condition multiple states cannot exist. An alternate film mechanism for this transition will be discussed below. However, the second transition is approximated reasonably well by the switching theory. Since the second transition takes place at a downflow rate less than the feed rate, in order to make comparisons it was necessary to recalculate δ_N and τ_0 on the basis of Q_D rather than Q_F and thus determine experimental values for the range of F, R_N and $(R_N)_{RMS}$ in order to make the comparison with theory.

The wave trace. This switching model suggests that the observed variation of film thickenss with time is the result of switching between various states of the system rather than the manifestation of the presence of large roll waves. Figure 10 is a section of a typical time trace of film thickness recorded at station A taken at the flooding condition for $Re_F = 310$ using test section configuration B. Figure 9 shows the theoretical solutions for δ vs τ_i for this flow rate. The vertical dashed lines represent the measured mean and shear and the range of shear as defined by $T_i \pm (\tau_i)_{RMS}$. The intersections with the curves represent the possible states of the system. A number of these states is located as horizontal lines on figure 10. Not only do these theoretical solutions effectively bound the observed thickness but repeated appearance of certain states is apparent. For example, the C state which represents zero wall shear stress is repeatedly observed. Other sections of the time trace for this same flow rate give similar results as do similar constructions made for the other three flow rates at the flooding condition. For the two higher flow rates this agreement is seen in each case only for the second of the transitions which, as discussed above, is the transition attributed to the switching mechanism. This result suggests that the large variations in amplitude of the film may be viewed as the result of arriving at different states rather than the existence of a well developed wave structure on the surface of the liquid film.

Wall shear stress. The switching theory can also explain the apparently anomalous values of wall shear stress observed at the flooding point. τ_w was calculated from measured

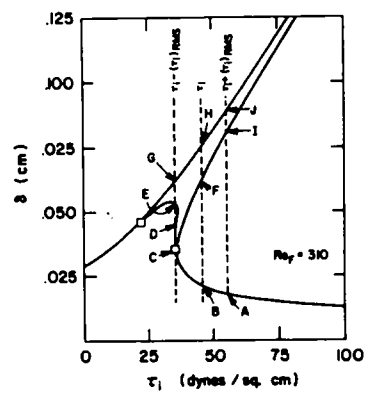

Figure 9. Location of steady states.

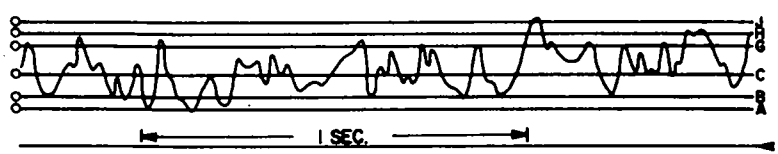

Figure 10. Wave trace compared with location of steady state.

values of film thickness and pressure gradient from

$$\tau_w = \left(\rho_L - \left|\frac{dp}{dx}\right|\right)\delta - \tau_i\left(1 - 2\frac{\delta}{D}\right). \quad [22]$$

For example, figure 11 shows values of τ_w for the falling film at $Re_F = 310$ calculated from experimental data. At the flood point the mean shear drops sharply to zero as shown. However, since the flow is downward at this condition, it is difficult to imagine a velocity distribution which could generate zero or negative wall shear. The concept of switching makes this understandable. Table 1 shows that the range of F at flooding for $Re_F = 310$ is 1.58–2.48. Identifying $F = 1.58$ with the curve OB of figure 7 and 2.48 with the curve UE and picturing the switching process suggest that the time average shear will be nearer the zero. The same conclusion is obtained at the flooding condition for other flow rates where the switching theory applies.

(B) *Kinematic wave model*

The transient behavior of two phase flow can be characterized by the time and space variation of the voids or the liquid holdup. Using ideas originally introduced by Lighthill & Whitham (1955), it will be shown that flow limitations can occur when the velocity of propagation of a kinematic wave becomes zero. The continuity equation for the liquid is

$$\frac{\partial}{\partial t}(1-\alpha)_x + \frac{\partial}{\partial x}[(1-\alpha)\bar{U}_L]_t = 0 \quad [23]$$

where α is the cross sectional average voids and $\bar{U}_L$ is the average film velocity. Note that $Q_L = (D/4)(1-\alpha)\bar{U}_L$ and the second term in [23] becomes $(4/D)(\partial Q_L/dx)_t$. The wall flow rate can be expressed as $Q_L = Q_L(\alpha, \tau_i)$ from which it follows that

$$\left(\frac{\partial Q_L}{\partial x}\right)_t = \left(\frac{\partial Q_L}{\partial \alpha}\right)_{\tau_i}\left(\frac{\partial \alpha}{\partial x}\right)_t + \left(\frac{\partial Q_L}{\partial \tau_i}\right)_\alpha \left(\frac{\partial \tau_i}{\partial x}\right)_t. \quad [24A]$$

But $\tau_i = \tau_i(\alpha, q_G)$ where q_G is the volumetric flow rate of gas. For constant q_G this equation becomes

$$\left(\frac{\partial Q_L}{\partial x}\right)_t = \left(\frac{\partial \alpha}{\partial x}\right)_t \left\{\left(\frac{\partial Q_L}{\partial \alpha}\right)_{\tau_i} + \left(\frac{\partial Q_L}{\partial \tau_i}\right)_\alpha \left(\frac{\partial \tau_i}{\partial \alpha}\right)_{q_G}\right\}. \quad [24B]$$

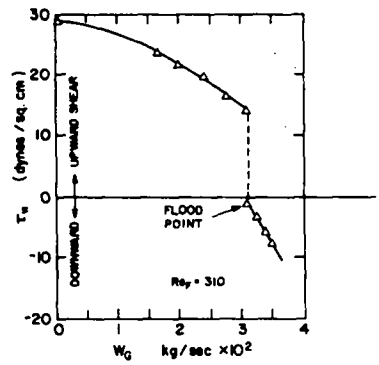

Figure 11. Variation of wall shear with gas rate.

Setting

$$C_K = -\frac{4}{D}\left[\left(\frac{\partial Q_L}{\partial \alpha}\right)_{\tau_i} + \left(\partial Q_L/\partial \tau_i\right)_{\alpha}\left(\frac{\partial \tau_i}{\partial \alpha}\right)_{q_G}\right]. \quad [25]$$

Then [23] can be written as

$$\frac{\partial}{\partial t}(1-\alpha) + C_K \frac{\partial}{\partial x}(1-\alpha) = 0 \quad [26]$$

where C_K is seen to be the downward velocity of propagation of a kinematic wave and [26] expresses the "conservation" of liquid holdup.

When C_K becomes zero then disturbances in $(1-\alpha)$ needed to accomodate random fluctuations in flow rate cannot propagate along the tube and flow limition or flooding can be expected to take place. Zuber (1964) applied the theory to dispersed two phase flow. In this paper its application to film flow is considered.

We search for the relationship between τ_i and δ dictated by the condition $C_K = 0$. $(\partial Q_L/\partial \alpha)_{\tau_i}$ and $(\partial Q_L/\partial \tau_i)_{\alpha}$ can be evaluated from [13]. The term, $(\partial \tau_i/\partial \alpha)_{q_G}$ can be found from

$$\tau_i = \frac{f_i}{2}\rho_G \bar{U}_G^2 = \frac{f_i \rho_G q_G^2}{2\alpha^2 A^2} \quad [27A]$$

and this gives

$$\left(\frac{\partial \tau_i}{\partial \alpha}\right)_{q_G} = -\tau_i\left[\frac{\partial f_i/\partial(\delta/D)}{4f_i\sqrt{\alpha}} + \frac{2}{\alpha}\right]. \quad [27B]$$

The result obtained after substituting for these partial derivatives into [25] and setting $C_K = 0$ is:

$$\tau_i = \frac{2\rho_L g D}{\frac{1}{f_i}\left[\frac{df_i}{d(\delta/D)}\right]_{q_G} + \frac{8}{1-2(\delta/D)} + \frac{2}{(\delta/D)}}. \quad [28]$$

Thus, the locus of points in the $\tau_i - \delta/D$ plane at which flooding takes place as a result of the inability to propagate a local change in film thickness is given by [28]. It is now clear that a quantitative description of this condition depends on the particular relationship which exists between f_i and δ/D as indicated by the first term in the denominator.

A variety of empirical equations have been proposed which related f_i and δ/D. However, as discussed in part I, these do not appear to describe the true behavior of the system. Their use in [28] cannot be expected to give realistic results. Instead, to test this idea, the experimental data in this study was used to estimate f_i vs (δ/D) along the flooding curve using [27A]. The results shown in figure 12 clearly reveals two different relationships for high and low rates respectively.

Now this information is used to determine if flooding takes place as a result of a limitation in the rate of propagation of a disturbance in liquid film thickness. Figure 13(A) shows the situation for the highest liquid rate. The solid curve, *N–O* corresponds to the same curve in figure 5, but in this case is presented in dimensional coordinates. It is the solution to the momentum equation for downflow. The dashed curve is a mapping of [28] (using figure 12 to find $df_i/d(\delta/D)$) and is the relation between δ/D and τ_i across which no propagation of liquid is possible. Now consider a small disturbance in δ/D.

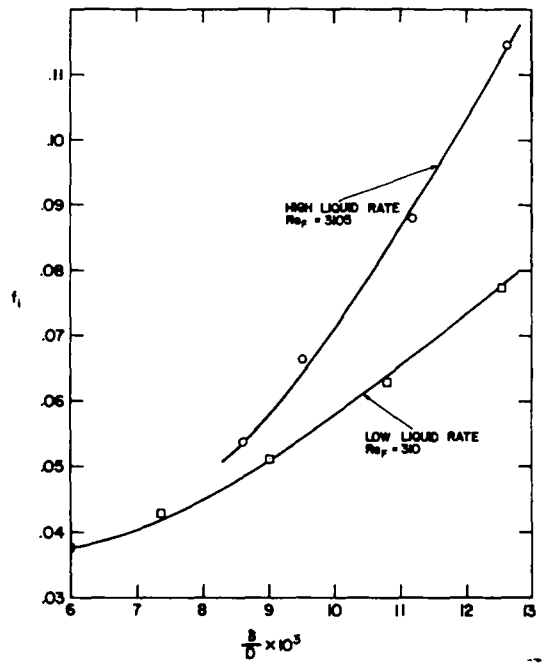

Figure 12. f vs δ/D along the flooding curve.

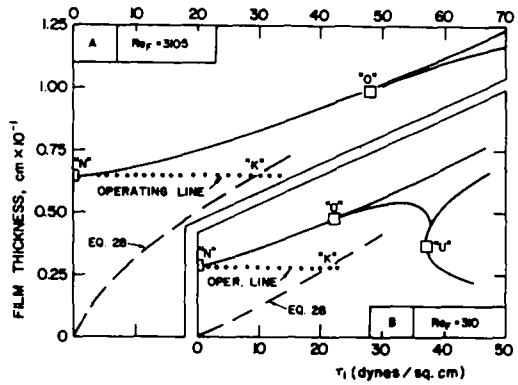

Figure 13. Flow limitations due to kinematic wave propagation mechanism.

Differentiating [27A] with respect to (δ/D) and substituting for $df_i/d(\delta/D)$ from figure 12 shows that this "operating" line relating δ/D and τ_i is essentially horizontal, shown as a dotted line. Thus, a very small disturbance in δ/D will result in a large change in τ_i. The process is pictured as follows. Just below the flooding point there occurs an increase in film thickness fluctuations as shown in figure 13, part I. This causes a sharp increase in shear stress as reflected by an increase in pressure gradient as shown in figure 7, part I. If τ_i is large enough to move the shear past the "O" point, then flooding takes place by the mechanism of multiple states as discussed above. However, if it is not large enough to exceed τ_0 but is large enough to intersect the curve for [28], shown as τ_K in the figure, then case shown in figure 13(A). Flooding must then initiate at the point of intersection between the operating curve, [27A], and the kinematic limiting curve, [28]. In fact, the theoretical value of $\tau_K \simeq 29$ dynes/cm. The value of τ_i for flooding measured experimentally is 28.5 dynes/cm.

A different situation is shown in figure 13(B) for the lowest liquid rate. Just before flooding in this case there is also a sharp increase in the film thickness fluctuation.

However, because this is taking place at a much higher gas rate, a larger $\Delta\tau_i$ results. In fact, at $Re_L = 310$, $\Delta\tau_i = 46$ dynes/cm. This increase carries the system well beyond the kinematic wave limiting condition at τ_K into the region of multiple states. Of course, if as a result of film thickness fluctuations $\Delta\tau_i$ is smaller than either τ_K or τ_0, then flooding does not occur.

It is of interest to notice the difference in the character of the film thickness curves for these two mechanisms. From figure 9, part I, it is seen that when the multiple states mechanism exists the film thickness increases sharply at flooding. When the kinematic wave limitation mechanism exists as for $Re_F = 3105$ then the film thickness decreases at flooding, as would be expected from the inability of the system to pass the liquid down.

SWITCHING THEORY APPLIED TO UPFLOW IN FILMS

It has long been recognized that there exists a serious discrepancy between the results of experiment and theory for upward film flow. Nicklin & Koch (1969) clearly demonstrated that measured film thicknesses were in poor agreement with the two theoretical solutions which would exist for any condition of interfacial shear. They described the agreement as hopeless!

Figure 14 shows the experimental data of this study for mean film thickness vs mean interfacial shear for concurrent upflow. Data for the four flow rates in test section configurations II and III (see figure 1, part I) are included. The solid curves represent the theoretical solutions for the four flow rates. There appears to be no way to explain this result except with the concept that the film thickness switches in order to satisfy the two possible solutions with the resulting mean value of the thickness falling between these two states of the system. Once again, this suggests that the *dominant* structure on the surface of the film is that due to the switching between states, not due to the presence of a well developed wave structure. Waves undoubtedly exist; however, the changes in amplitude associated with switching are large compared with that due to wave motion and as a result true wave action will not be observed until the film becomes thin and the amplitude of the switching is small.

Support for this conclusion comes from several types of circumstantial evidence. Just

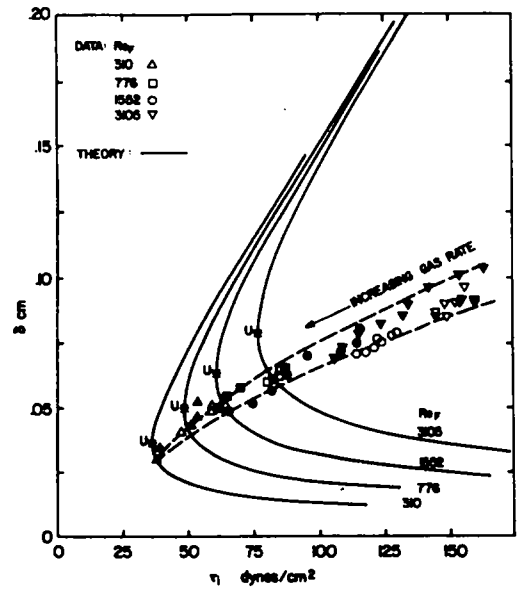

Figure 14. Mean film thickness compared to theory for upflow film (open symbols are for test section II, closed for III).

at the flooding point the film thickness and the pressure gradient are high (see figures 7 and 10, part I). As the gas rate is increased both of these quantities decrease. Thus, the data of figure 14 tends to the left and downward as indicated by the arrow with increasing gas rate. A study of the film thickness fluctuations as shown in figure 14, Part I shows that the RMS film thickness fluctuation is likewise largest for the data at the lowest gas rates and decreases with increasing gas rate, just as the switching model would predict and with the correct order of magnitude of fluctuation.

The dominance of the switching at lower gas rates is also evident from studies of cross covariance of the film thickness. These measurements were carried out in test section configuration C between stations B and C located 0.16 m apart (see part I, figure 1). The cross covariance function is defined as

$$\rho_{BC}(\tau) = \frac{\operatorname{Lim}_{T\to\infty} \frac{1}{T}\int_0^T \delta'_B(\tau)\delta'_C(t+\tau)\,dt}{(\delta'_B)_{RMS}(\delta'_C)_{RMS}}$$

where

$$\delta'(t) = \delta(t) - \langle\delta\rangle$$

$$\langle\delta\rangle = \operatorname{Lim}_{T\to\infty} \frac{1}{T}\int_0^T \delta(t)\,dt$$

$$(\delta'_{RMS})^2 = \operatorname{Lim}_{T\to\infty} \frac{1}{T}\int_0^T (\delta')^2\,dt$$

and τ is the delay time. Typical results for four gas rates at each of the four experimental liquid feed rates appear in figures 15–18. In each case, curve A represents the gas rate at flooding, the point at the furthest right for that liquid rate on figure 14. Curve D represents the highest gas rate and is the point furthest to the left for that liquid rate in figure 14.

A wave mechanism for flooding in which well developed roll waves move upward should result in a well defined peak in the cross covariance located at a delay time, τ, equal to the time it takes the wave to travel between the two stations. However, a study of figures 15–18 show that such peaks are not present for curves A and B which essentially span the range of flow rates from the start of flooding to all upflow. In these curves the normalized standard error is estimated to be 0.032 and peaks falling in the amplitude range 0.064

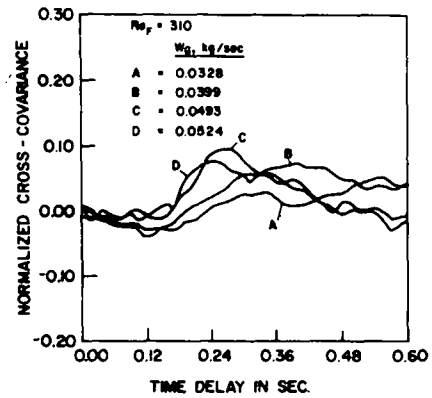

Figure 15. Cross covariance data (stations B and C, test section III).

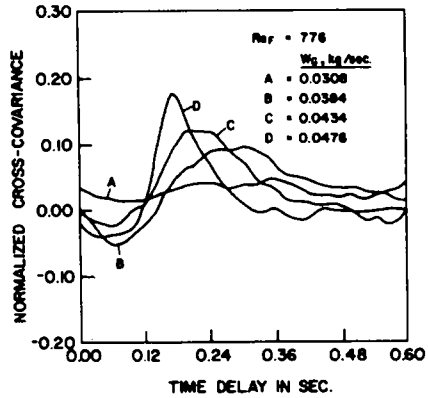

Figure 16. Cross covariance data (stations *B* and *C*, test section III).

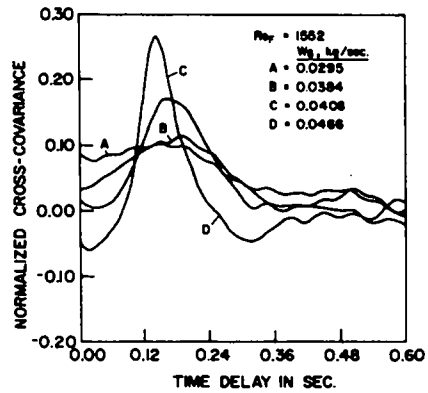

Figure 17. Cross covariance data (stations *B* and *C*, test section III).

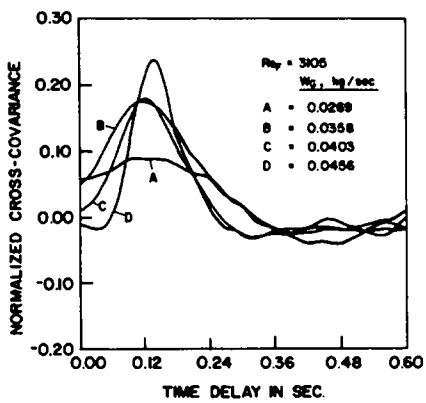

Figure 18. Cross covariance data (stations *B* and *C*, test section III).

cannot be considered statistically significant. At higher gas rates where uniform upflow of the film takes place (curves *C* and *D*) the presence of waves travelling upward is clearly indicated by well defined peaks. In contrast, a mechanism based on random switching between the multiple possible states of the system can be expected to result in a cross covariance that is distributed more uniformly over all delay times precisely as shown by these curves over the range of flooding and flow reversal (curves *A* and *B*).

Hewitt *et al.* (1965) demonstrated that for concurrent upflow of climbing films the pressure gradient displays a minimum with increasing gas rate and that the fluctuations in film thickness were greatest at the lowest gas flow rates just at transition and were

significantly less for gas rates above the minimum. This suggests the path of the system to be that shown in the sketch of figure 19. The first section of the data fall inside the upflow loop *CUE* with switching taking place between the two states and the mean film thickness approaching the intersection of the two branches at *U* as the gas rate increases. As a result, the film thicknesses in the two states approach one another and the fluctuations decrease. As the gas rate is increased further, the system follows the uniform upflow branch along *UE* with the shear increasing and the film thickness decreasing and displaying only smaller fluctuations as observed from experiment. Along this branch the fluctuations are caused by the waves which exist on the surface.

Further evidence for this switching theory is provided by a study of wall shear stress as calculated from the data compared to theoretical values. Figure 20 is an exapanded view of the ratio of wall shear stress to the Nusselt value for the same liquid flow rate in the film. The theoretical expression for this quantity is

$$\frac{\tau_w}{\tau_{wn}} = \phi R_N \left[1 - \sqrt[3]{0.5} \frac{F}{R_N} \frac{\phi_0^{2/3}}{\phi} \right] \qquad [29]$$

and this has two branches because for each F there are two values of R_N.

Values of the time average τ_w were computed from the time average film thickness and pressure gradient data using [22]. At each experimental point the upflow rate in the film is known so that δ_N and τ_{wn} can be calculated. The resulting experimental data are shown as symbols. It is clear that on average the shear stress is negative (downward directed).

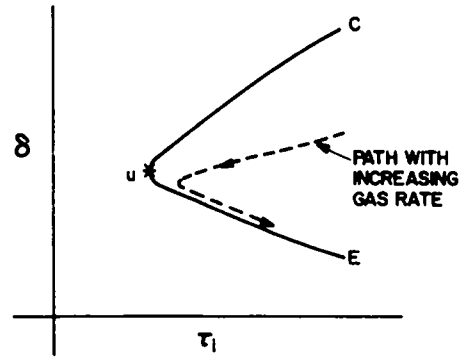

Figure 19. Path in the δ-τ_i plane.

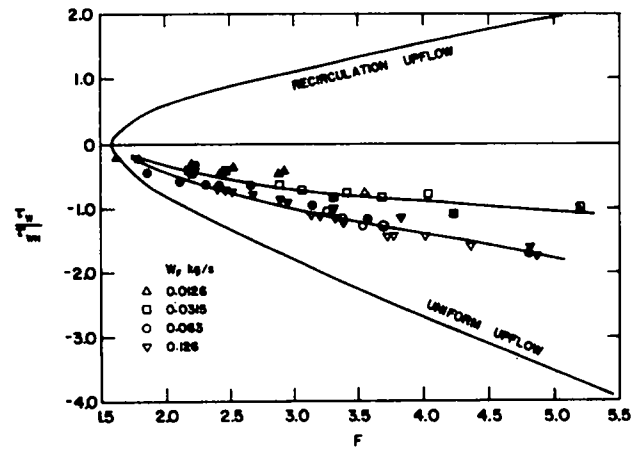

Figure 20. Dimensionless wall shear stress for upflow (open symbols are for test section II, closed for III).

However, the mean experimental values which are measured to fall withing the loop can be explained only if conditions switch between several possible states of the system. In fact, these data suggest that the states oscillate between uniform upflow and the "U" state where the wall shear is zero. A reasonable estimate of τ_w/τ_{ww} is the arithmetic average of the two ratios of any F.

In part I experimentally determined values of wall friction factor are reported. It is now possible to explain these anomalous trends of the results. From the definition of friction factor and the theoretical expression for wall shear,

$$\tau_w = \phi S_L g \delta \left[1 - \sqrt[3]{0.5} \frac{F}{R_N} \frac{\phi_0^{2/3}}{\phi} \right] \qquad [30]$$

the following expression is derived

$$f_w = \frac{24}{\mathrm{Re}_L} \psi(F) \qquad [31]$$

where

$$\psi(F) = \frac{1 - \sqrt[3]{0.5} \dfrac{F}{R_N} \dfrac{\phi_0^{2/3}}{\phi}}{1 - \dfrac{3}{4} \sqrt[3]{\dfrac{4}{\phi_0}} \dfrac{F}{R_N}}. \qquad [32]$$

Now it is seen that for liquid films f_w depends on both the liquid Reynolds number and the dimensionless interfacial shear, F. For upflow there are, of course, two values of f_w for each F corresponding to the two values of R_N. Thus for each Re_L there is a range of values within which f_w can fall. Figure 21 shows curves for f_w vs Re_L for two liquid feed rates taken from figure 20, part I. Values of F were determined from experiment along the curve and these were used to calculate the bounds of the possible values of f_w. The result shows that the theoretical values bound the experimental ones. It further shows that for films,

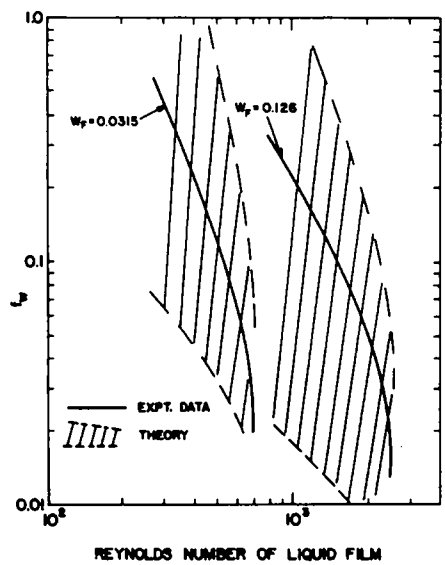

Figure 21. Wall friction factor comparison of theory and experiment.

the concept of friction factor is not a particularly useful one to calculate wall shear. Clearly, study must now be directed to the dynamics of the switching process.

CONCLUSIONS

Three new mechanisms for flooding are considered in this paper: (a) Flooding takes place as a result of switching between stable states of the system some of which cause upflow. The extent of upflow depends on the fraction of time the system is in the upflow state. This model is consistent with measured values of mean and RMS film thickness, the characteristics of the film thickness time trace and measured values of wall shear stress. (b) Flooding takes place as a result of the system exceeding the propagation velocity of a kinematic wave. (c) Flooding takes place as a result of entrainment. The mechanism which controls in any given application is the one which is reached first as the gas rate is increased. Other mechanisms may also be operative.

The idea of switching is suggested as an explanation to explain anomalous results on the film thickness for upward concurrent film flow.

Acknowledgements—The financial support of the U.S. Nuclear Regulatory Commission for both the theoretical and experimental work is gratefully acknowledged. Numerous conversations with Dr. Novak Zuber were particularly helpful in crystallizing some of these ideas. Suggestions by Dr. G. F. Hewitt were important to the presentation.

REFERENCES

CENTINBUDAKLAR, A. G. & JAMESON, G. J. 1969 The mechanism of flooding in vertical countercurrent two phase flow. *Chem. Engng Sci.* **24**, 1669–1680.

DUFFEY, R. B., ACKERMAN, M. C., PIGGOTT, B. D. G. & FAIRBAIRN, S. A. 1978 The effects of countercurrent single and two phase flows on the quenching rate of hot surfaces. *Int. J. Multiphase Flow* **4**, 117–140.

DUKLER, A. E. 1977 The role of waves in two phase flow: some new understandings. *Chem. Engng Educ.* **11**, 108.

DUKLER, A. E. & SMITH, L. 1977 Two phase interactions in countercurrent two phase flow: Studies of the flooding mechanism. *U.S. Nuclear Regulatory Commission Report, NUREG/CR-0617.*

FEIND, K. 1960 Falling liquid films with countercurrent air flow in vertical tubes. *VDI Forschungshft* **26**, 5.

HEWITT, G. F. & WALLIS, G. B. 1963 Flooding and associated phenomena in falling film flow in a tube. *UKAERE Report R-4022.*

HEWITT, G. F., LACEY, P. M. C. & NICHOLLS, B. 1965 Transitions in film flow in a vertical tube. *Proc. Two Phase Flow Conf.*, Exeter, England.

HEWITT, G. F. 1977 Influence of end conditions, tube inclination and fluid physical properties on flooding in gas–liquid flows. *UKAERE Heat Transfer and Fluid Flow Service Report HTFS-RS* 22.

HEWITT, G. F. & WHALLEY, P. B. 1980 Advanced optical instrumentation methods. *Int. J. Multiphase Flow* **6**, 139–156.

IMURA, H., KUSADA, H. & FUNATGU, S. 1977 Flooding velocity in a countercurrent annular two phase flow. *Chem. Engng Sci.* **32**, 79–87.

LIGHTHILL, M. H. & WHITHAM, G. F. 1955 On kinematic waves. *Proc. Roy. Soc.* **229**, 281.

NICKLIN, D. J. & KOCH, B. E. 1969 A model of two phase annular flow. *Concurrent Gas–Liquid Flow* (Edited by RHODES & SCOTT). Plenum Press, New York.

PUSHKIN, O. L. & SOROKIN, Y. L. 1969 Breakdown of liquid film motion in vertical tubes. *Heat Trans.-Soviet Res.* **1**(5), 56–94.

RICHTER, H. J. 1981 Flooding in tubes and annuli. *Int. J. Multiphase Flow* **7**, 647–658.

SCHUTT, J. B. 1959 A theoretical study of the phenomenon of bridging in wetted wall columns. B.S. Thesis, Univ. of Rochester.

SEVIK, M. & PARK, S. H. 1973 The splitting of drops and bubbles by turbulent fluid flow. *Trans. ASME, J. Fluids Engng* **95**, 53.

SHEARER, C. J. & DAVIDSON, J. F. 1965 The investigation of a standing wave due to gas blowing upward over a liquid film: its relation to flooding in wetted wall columns. *J. Fluid Mech.* **22**, 321–335.

SOLEVEV, A. V., PREOBRAZHENSKII, E. I. & SEMENOV, P. A. 1967 Hydraulic resistance in two-phase flow. *Int. Chem. Engng* **7**(1), 59.

SUSUKI, S. & UEDA, T. 1977 Behavior of liquid films and flooding in countercurrent two phase flows—I. Flow in circular tubes. *Int. J. Multiphase Flow* **3**, 517–532.

TAITEL, Y., BARNEA, D. & DUKLER, A. E. 1982 A film model for prediction of flooding and flow reversal for gas–liquid flow in vertical tubes. *Int. J. Multiphase Flow* **8**, 1–100.

TIEN, C. L. & LIU, C. P. 1979 Studies on vertical two phase countercurrent flooding. *Electric Power Research Institute Report NP-984.*

ZUBER, N. 1964 On dispersed two phase flow in the laminar flow regime. *Chem. Engng Sci.* **19**, 897.

ZVIRIN, Y., DUFFY, R. B. & SUN, K. H. 1979 On the derivation of a countercurrent flooding theory. In *Fluid Flow and Heat Transfer Rod and Tube Bundles* (Edited by S. C. YAO & P. A. PFUND). Papers presented at the ASME Winter Annual Meeting, 111–119.